Recombination lasing in a magnetoplasmadynamic arcjet

E. M. Campbell,[a] R. G. Jahn,[b] W. F. von Jaskowsky,[c] and K. E. Clark[d]
Princeton University, Princeton, New Jersey 08544

(Received 3 May 1979; accepted for publication 24 August 1979)

The plasmadynamic recombination laser concept is verified experimentally in a high-power quasisteady MPD arcjet operating at 4 kA and 12 g/sec of argon. Measurements of the spatial variation of electron temperature, electron density, and population densities in the arc exhaust flow confirm that inverted populations of the $4p$ to $4s$ Ar II transitions are established by collisional-radiative recombination of the Ar III ion. Using an optical cavity aligned transversely to the flow, recombination lasing of seven such transitions, 5145, 4880, 4764, 4727, 4658, 4579, and 4545 Å, is observed spectrophotograpically and photoelectrically over the entire 1-msec discharge.

PACS numbers: 42.60.By, 52.30. + r, 34.90. + q, 42.55.Fn

I. BACKGROUND

The concept of a recombination laser was first introduced by Gudzenko and Shelepin in 1963.[1] In lasers of this type, population inversions of electronic states of atoms or ions in a plasma are created during ionization recombination following a nonequilibrium cooling process. The use of a recombining plasma as an amplifying medium for electromagnetic radiation offers several potential advantages. (1) since the mechanism is applicable to many electronic transitions in a broad variety of atomic and ionic species, there exists the possibility of lasing from the infrared to soft x-ray regions of the spectrum; (2) lasing may be realized in both cw and pulsed modes; (3) because of the inherently high-energy capacity of discharge plasmas, lasers with high-energy and/or high-power output may be feasible.

The amplifying medium in a recombination laser is an "overionized" plasma in which the free-electron number density is appreciably greater than the Saha value for the local electron temperature.[2] This distinguishes recombination lasers from the more widely known electric discharge lasers, such as the conventional argon ion laser, which also employ nonequilibrium plasmas as the active media.[3] In such electric discharge lasers, the free-electron number densities are less than the Saha value for the local electron temperature. Recombination lasers thus are characterized by plasmas of higher density and lower temperature than the more familiar electric discharge lasers.

In recombining plasmas, the populations of the atomic states are determined by collisional-radiative recombination involving the next-higher ionic state and the free electrons. As described by Bates *et al.*,[4] collisional-radiative recombination includes both the initial capture of the free electrons and all subsequent bound-bound (and possible bound-free) collisional and radiative transitions that affect the captured electrons as they migrate downward through the energy structure of the atomic or ionic species. For sufficiently dense plasmas, the initial capture of the electron is achieved via a three-body interaction among an ion-electron pair and a second free electron. The recombined atom or ion is normally left in a highly excited energy state with a binding energy of the order of the mean electron thermal energy kT_e or less, and the balance of the energy liberated in the collision is transferred mainly to the free electron. The atom or ion subsequently relaxes to lower-lying energy states, at first primarily via superelastic collisions and then, depending on the detailed structure of its energy levels, and the plasma environment, by a combination of superelastic collisions and spontaneous radiative decay.

The low-lying states are initially underpopulated since: (1) the initial recombination preferentially feeds the high-lying states; (2) collisional pumping from the ground state is unimportant at the low electron temperature; (3) the low-lying states decay more rapidly by spontaneous emission (provided radiation transfer effects can be ignored).

This general collisional-radiative process does not guarantee that a population inversion will be formed. In order to achieve lasing for a time scale longer than the characteristic relaxation time of an excited atomic state ($\approx 10^{-8}$ sec), it is also necessary that the lower-energy state of the particular lasing transition be depopulated at a rate faster than that of the upper state. This depopulation process can proceed either by radiative decay or by electron or heavy particle collisional deactivation. For example, the former process has been shown to generate inversions in certain recombining hydrogen plasmas,[5] whereas electron collisional deactivation was found to be the predominant mechanism for forming inversions in recombining lithium plasmas.[6] Thus, in a recombination laser, the upper level is fed by a cascade originating in the continuum, and the lower level is preferentially depopulated by selective radiative or collisional processes.

Because of the importance of the quantum structure of the atom in determining the feasibility of a recombination laser, a theoretical analysis of the amplifying medium must include the population kinetics of a multilevel system, a diffi-

[a] Graduate Student, Mechanical and Aerospace Engineering Department, Princeton University, Princeton, N.J.
[b] Dean, School of Engineering and Applied Sciences, Princeton University, Princeton, N.J.
[c] Senior Research Engineer and Lecturer, Princeton University, Princeton, N.J.
[d] Research Engineer, Princeton University, Princeton, N.J.

 0021-8979/80/010109-09$01.10

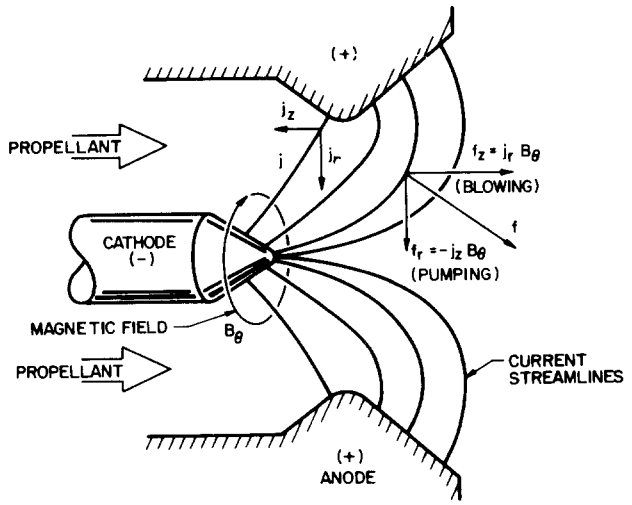

FIG. 1. Self-field MPD accelerator.

cult problem which is aggravated by the lack of reliable data on the rates of many elementary processes. Primarily because of this difficulty, the majority of the theoretical treatments of recombining plasmas, and to a certain extent the experiments as well, have been confined to species of simple atomic structure. Detailed calculations for recombining hydrogen,[5] hydrogenic,[7] lithium,[6] and potassium[8] plasmas confirm that population inversions large enough to allow laser oscillation can be established within certain ranges of electron density and temperature. Theoretical treatments for nitrogen and xenon plasmas using simplified energy-level structures for the atoms have also indicated the feasibility of establishing such an amplifying medium in more complex atomic systems.

One of the main tasks for the experimental demonstration of a recombination laser is the attainment of the indicated combinations of electron temperatures and densities by some mixed cooling mechanism wherein the degree of ionization lags appreciably above the Saha value for the local electron temperature. Many techniques have been attempted to achieve this.[2] For example, several authors have examined the nonequilibrium decay of electric discharge afterglows,[9,10] wherein the electrons are cooled by the walls, by heavy particle collisions, or both. The first thorough study of this type of recombination laser was achieved in Mg II, Ca II, Sr II, and Ba II in the infrared, visible, and uv regions of the spectrum during the afterglow of a high-voltage longitudinal field pulsed discharge. A maximum output power of 50 W was reported for the 4305-Å line of Ca II. Such afterglow lasers are attractively simple to operate, but they are inherently short pulse devices ($\simeq 10^{-6}$ sec) and do not seem to be easily scaled to high-energy output.

The requisite plasma environment can also be created through the use of external ionization sources such as electron beams or fission fragments from nuclear reactors.[11,12] The advantage of this technique is the decoupling of plasma production from the electron kinetics, which allows the formation of a dense plasma with a low electron temperature.

A rapid expansion and accompanying nonequilibrium plasma relaxation can also lead to recombination lasing. Silfvast *et al.*[13] observed lasing action in the near infrared from expanding Ar, Xe, and Kr plasmas created in the far field of a cylindrically focused pulse CO_2 laser. A peak power of 250 W was obtained with xenon. Inversions in highly stripped recombining aluminum also have been observed in the expanding plasma formed from the irradiation of a high-power, pulsed Nd : glass laser.[14]

As one method of achieving steady recombination lasing, several authors[7,8,15,16] have suggested the use of arcjets or plasma jets to provide steady or quasisteady expanding plasma flows of the proper species and temperature profiles. In such steady plasmadynamic lasers, the flow is first heated and ionized in an arc chamber and then cooled by exhausting the flow into a suitable vacuum chamber. Properly tailored, this exhaust flow may provide a propitious medium for cw laser operation at large output powers. While several experimenters have reported inverted populations in such recombining hydrogen, helium and argon plasma jets,[15-17] to our knowledge none had achieved sufficient small gain to sustain actual laser oscillation prior to these experiments.

In this paper, we describe the results of a series of experiments designed to examine the recombination process in the argon exhaust flow of a high-power quasisteady magnetoplasmadynamic (MPD) arcjet. The identification of significant ionizational and electronic nonequilibrium in the rapidly expanding plasma flow leads to a cavity experiment in which lasing is observed over the 1-msec operating time of the accelerator. We believe this to be the first quasisteady plasmadynamic laser, i.e., a laser driven by steady recombination pumping in an expanding plasma flow.[18,19]

II. EXPERIMENTAL APPARATUS

A. MPD facility

The MPD arc is a plasma accelerator, particularly well suited to this application. In its most common form, it consists of a coaxial electrode arrangement like that shown schematically in Fig. 1, through which currents greater than 10^3

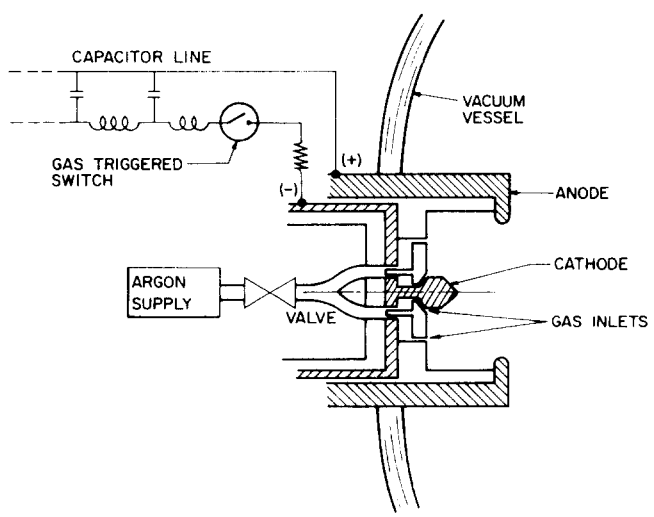

FIG. 2. MPD discharge apparatus.

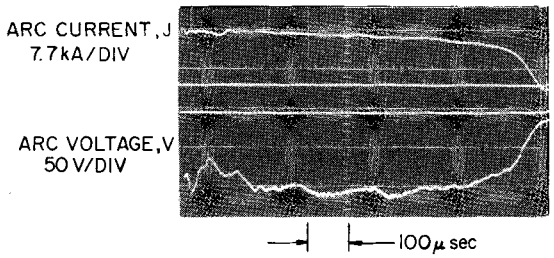

FIG. 3. Current and voltage signatures.

A and mass flows greater than 1 g/sec are passed.[20-22] The plasma created in the arc chamber is both compressed and accelerated by Lorentz body forces arising from the interaction of the arc current with the self-generated azimuthal magnetic fields, and then is cooled by expansion through the anode orifice, usually into a vacuum vessel.

Since the acceleration process, and hence the compression and expansion, intensify disproportionately with arc power, there is benefit in operating such arcs at very high currents. These are most comfortably handled in the laboratory in a "quasisteady" mode of operation, wherein up to 10^5 A may be driven for times of the order of 1 msec.[23,24] Using this approach, arc operation in the range from 10^5 to 10^7 W can be attained with relatively modest power sources, and without serious heat transfer or gas-handling problems. Of particular interest for plasmadynamic laser studies, flows of substantial energy density can be extracted from such quasisteady devices, with dimensions an order of magnitude greater than conventional steady-flow arcjets, thereby providing correspondingly longer optical paths which reduce the threshold inversion density required for laser oscillation.

The quasisteady MPD accelerator used for the present experiments is shown schematically in Fig. 2. A 12.7-cm-diam by 5.1-cm-deep cylindrical arc chamber is formed by an aluminum anode with a 10.2-cm-diam orifice, a conical tip tungsten cathode with a base diameter of 2 cm, and appropriate side and rear insulators.[25] A rectangular current pulse from 4 to 21 kA and up to 1-msec duration is delivered to the electrodes by a 160-kJ capacitor bank arranged in an *LC* ladder network.[26] Argon mass flow is injected through a boron nitride backplate via a high-speed solenoid valve. This and previous studies have shown that all electrical and gas-dynamic transients subside by about 100 μsec after discharge initiation, leaving a steady highly ionized plasma outflow at velocities of the order of 10^4 m/sec for the remainder of the pulse.[25] An oscillogram of typical current and voltage signatures of the MPD discharge is shown in Fig. 3.

B. Diagnostics

1. Electrostatic probes

Symmetric cylindrical double electrostatic probes are used to measure the electron density and temperature profiles in the exhaust flow of the accelerator. The tungsten electrodes of these probes are typically 7.6×10^{-3} cm in diameter and 0.76 cm in length, with a spacing of 0.5 cm. Electron temperature and number density are reduced from the probe characteristic using the theories of Johnson and Malter,[27] Chen,[28] and Laframboise.[29]

Given the short duration of the plasma flow and the large number of locations to be sampled, it is beneficial to use a special probe biasing circuit which can generate its entire current-voltage characteristic in one firing of the accelerator. The voltage biasing unit is capable of providing either a free-running sawtooth waveform or just one to four segments of this waveform. The amplitude can be varied from -20 to $+20$ V, the sweep time per segment can be as short as 50 μsec, and in the partial segment mode, the time of voltage sweep initiation can be delayed with respect to an initial timing mark.

A schematic illustration of the double-probe circuitry is shown in Fig. 4. The probe voltage sweep is triggered by a pulse generator delayed several hundred microseconds with respect to discharge initiation to guarantee steady plasma conditions at the probe location. For most of the data reported here, only one linear ramp segment of the sawtooth is used, i.e., the circuit maintains a constant negative bias on the probes until triggered, at which time it sweeps to a bias of

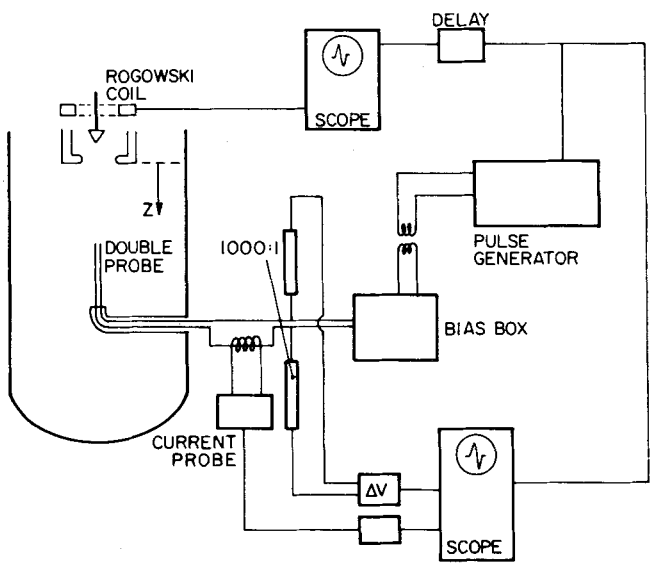

FIG. 4. Probe circuitry.

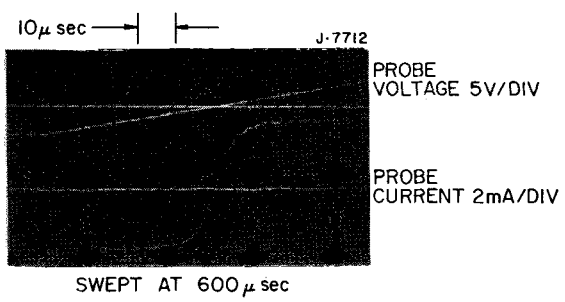

FIG. 5. Probe characteristic.

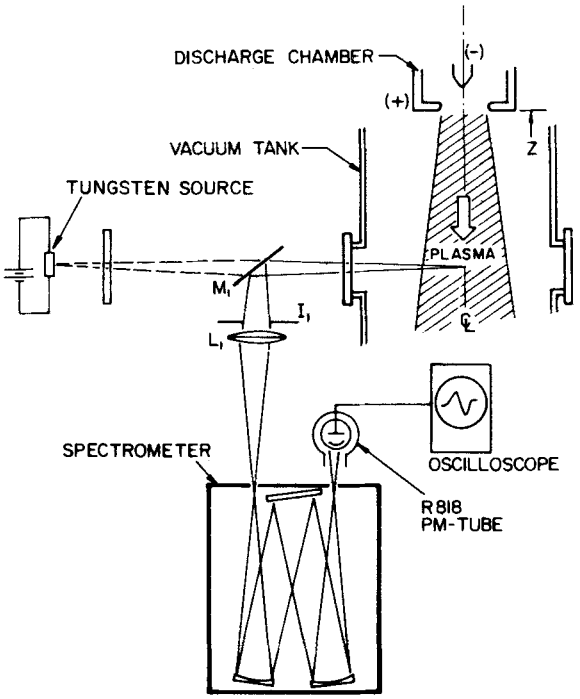

FIG. 6. Optical arrangement.

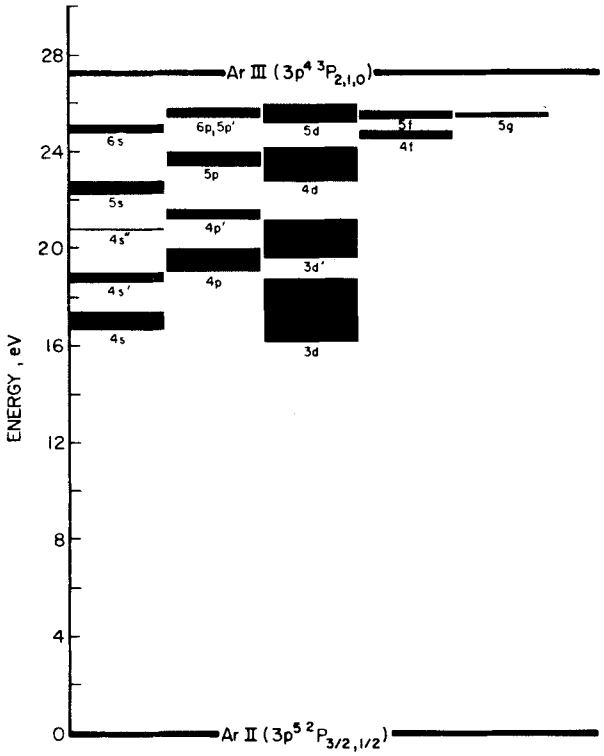

FIG. 7. Argon II Grotrian diagram (simplified).

equal amplitude but opposite sign. In separate experiments the voltage sweep rate has been shown not to affect the probe characteristic.[30]

Figure 5 shows a typical record of the probe voltage and current over a 100-μsec interval during which the bias is swept from -4 to $+4$ V. Because the voltage increases linearly in time, the lower trace represents the current-voltage characteristic of the probe multiplied by a constant scale factor which depends on the voltage amplitude and sweep rate.

2. Radiance measurements

The emission spectra and absolute plasma radiance necessary for determination of species distributions and population densities are obtained using the optical system shown schematically in Fig. 6. Spectrograms in the ultraviolet, visible, and near-infrared wavelength regions are recorded using a Spex 0.75-m spectrometer with a plane diffraction grating of 1200 rules/mm, 56-cm^2 effective area, blazed for 7500 Å. This spectrometer has a nearly constant inverse linear dispersion of 10.9 Å/mm over the entire wavelength range and an effective f number of $f/10$.

The spectrometer may also be operated in a monochromator mode by inserting narrow adjustable slits at the exit focal plane. A Hamamatsu R818 photomultiplier tube of S-20 special response with extended uv sensitivity is placed behind the exit slits to detect the plasma radiance. For absolute measurements in the visible and near infrared, the entire optical system is calibrated with a standard tungsten source.

With this optical system, the population densities of excited electronic states may be determined from the line intensities, provided the plasma is optically thin to the radiation.[31] For the majority of the transitions of interest, the optical depth was measured to be of the order of 10^{-2}, so that the total line intensities I_{ji} may be expressed as the path integral of the local emission coefficients ϵ_{ji}, which in turn are proportional to the upper state population densities n_j:

$$I_{ji} = \int_0^L \epsilon_{ji}\, dx\,, \tag{1}$$

$$\epsilon_{ji} = (h\nu_{ji}/4\pi)A_{ji}n_j\,. \tag{2}$$

Since the exhaust flow is cylindrically symmetric, further reduction of the data using an Abel inversion technique is possible, yielding local values of the emission coefficients and number densities.

The magnitudes of the necessary Einstein coefficients A_{ji} are either found in the literature or calculated using the coulomb approximation of Bates and Damgaard.[32] For reference, a simple Grotrian diagram of Ar II is shown in Fig. 7 with the energy states involved in this study labeled by the

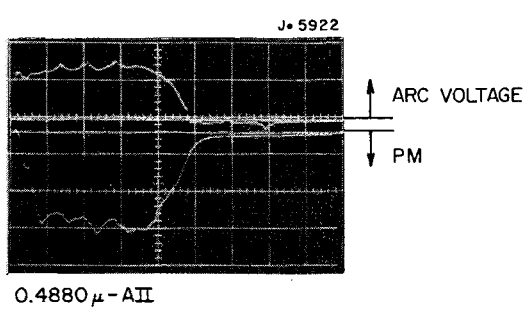

FIG. 8. PM response.

appropritae electronic configurations.[33] The shaded regions encompass the many closely spaced fine-structure levels.

As one example of a typical optical measurement, the lower trace of Fig. 8 shows the phototube response to a $4p$-$4s$ Ar II transition (4880 Å); the upper trace of Fig. 8 is the accelerator terminal voltage. From the quasisteady amplitude of the lower signal and the calibrated optics, the population of the particular upper state, in this case $3p^4(^3P)4p\ ^2D^0_{5/2}$, can be determined.

3. Laser cavity

The resonant optical cavity in which lasing has been demonstrated may be installed at various axial positions downstream of the accelerator, as shown schematically in Fig. 9. The cavity is formed by two spherical mirrors, each of a radius of 147 cm, placed outside of the vacuum vessel at a separation of 140 cm. The cavity is stable, and the Fresnel number of the mirrors is 45, so that diffraction losses for the TEM_{00} mode are negligible.[34] The reflectivity of one mirror exceeds 99.5% and the output coupler has a transmission of 3% in the wavelength region of interest. The useful wavelength range of the mirrors is $4500 \leqslant \lambda \leqslant 5200$ Å, which overlaps the wavelength region of the predominant $4p$-$4s$ Ar II emission lines. Optical coupling of the plasma region to the mirrors is via Brewster windows inserted in the walls of the vacuum vessel. No special effort is made to optimize the output coupling or to maximize the active medium volume. Appropriate optics direct the cavity output into the spectrometer and the optical signal is recorded either with a photomultiplier tube or on film.

C. Properties of the plasma flow

Using the experimental devices and techniques described in Sec. II B, various properties of the MPD exhaust plume have been mapped to establish its state and composition during the expansion process, and from these to deduce the principal recombination mechanisms. From the excited-state population density measurements, inversions are suggested and used as a basis for selecting the location for the optical cavity experiments to follow. Unless otherwise specified, the accelerator operating conditions for these data are fixed at a current of 4 kA and a mass flow of 12 g/sec.

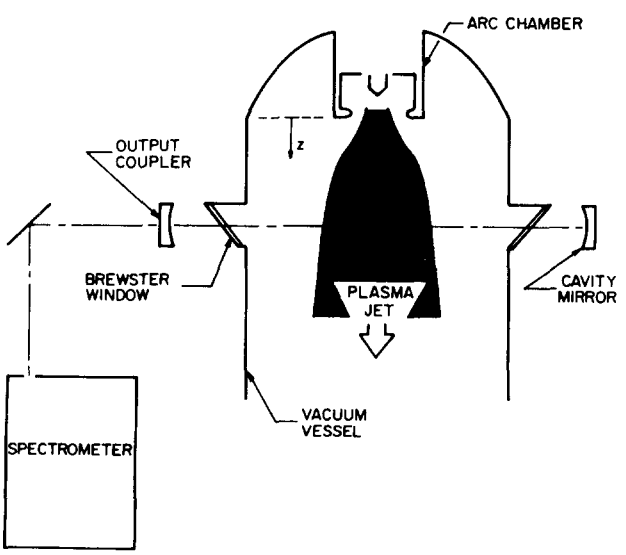

FIG. 9. Plasmadynamic laser arrangement.

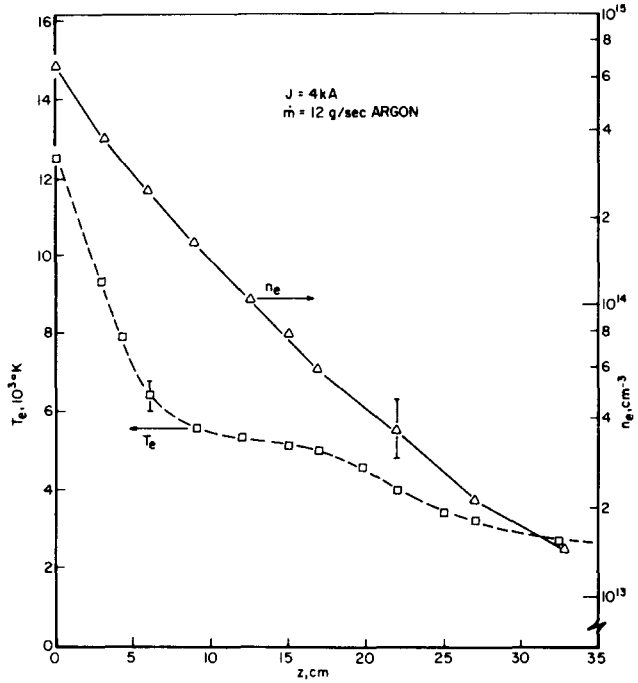

FIG. 10. Centerline electron temperature and density.

D. Electron temperature and density

The experimentally determined profiles of electron temperature and number density along the plume centerline ($r = 0$) are shown in Fig. 10, where the origin of the axial or z coordinate is located at the anode plane. The electron temperature is seen to decay rapidly from 12 500 ° K at the anode plane to 5400 ° K 10 cm downstream. This rapid decay is followed by a nearly constant temperature region extending another 10 cm and then by a region of further decay until T_e reaches some 2400 ° K, 36 cm from the anode. Electron temperature within the arc chamber itself is much more difficult to determine because of the high plasma density there, but probe data obtained near the cathode tip, about 2 cm upstream of the anode, indicate $T_e \approx 25\,000$ ° K.

The profile of electron density is also plotted in Fig. 10 and shows a monotonic decrease with axial distance from 6×10^{14} cm^{-3} at the anode to 10^{13} cm^{-3} at $z = 36$ cm. No immediate transcription of this electron density decay to an electron-ion recombination rate is possible because the expansion of the plasma cannot be adequately described by any simple fluid mechanical model, such as a source flow expansion from a sonic orifice.[25]

The radial profile of electron temperature is also of interest for laser considerations because the magnitude and sign of the amplification coefficient for a particular transition results from an integration of the population densities along the optical axis, in this case the radial direction. In Fig. 11 the measured radial profiles of electron temperature are

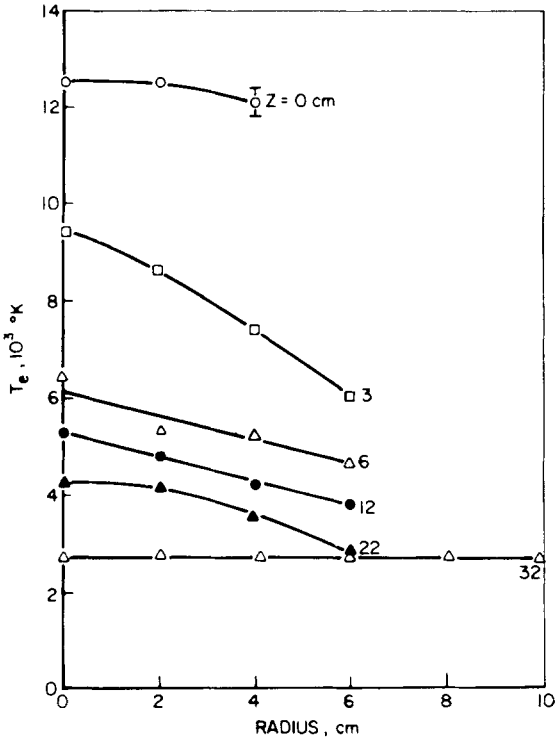

FIG. 11. Radial profiles of electron temperature; $J = 4$ kA, $\dot{m} = 12$ g/sec.

shown at various axial stations. The data show that at downstream positions beyond 10 cm, the T_e value drops only about 20% from the centerline out to a radius of 6 cm, the largest radius at which reproducible data can be obtained, and the visible edge of the plume.

From the measured centerline values of n_e and T_e it can be concluded that the electron-ion recombination process in the plume begins with a three-body electron capture. Figure 12 shows regions of the n_e-T_e plane where two-body (radiative) and three-body recombination dominate, computed from the relations given by Pitaevskii[35] and Zel'dovich and Raizer.[36] (Molecular recombination processes, i.e., dissociative recombination, can be shown to be negligible for this argon plasma.) Data for the present experiments are contained within the unshaded region, well within the three-body recombination domain. This situation is essential for recombination laser operation since the rate of two-body recombination directly into the ground state of the atom or ion approximately equals that into all other states combined. Consequently, no inversions can be created by two-body recombination, in contrast to three-body collisional recombination which preferentially feeds the high-lying energy states.

E. Exhaust plume spectra

Spectra of the plasma jet taken over the wavelength ranges from 2000 to 8500 Å, and over axial positions from $z = 1$ to 45 cm, are used to determine the dominant radiating species in the exhaust and to obtain qualitative information on the axial decay of the plasma. This wavelength range contains a large number of strong emission lines from the neutral, first, and second ion argon spectra, and possible impurity lines from insulator ablation (boron, nitrogen) and electrode erosion (tungsten, aluminum).[37] No spectra can be obtained with our equipment covering the resonant transitions of Ar I, Ar II, and Ar III, which lie in the 400–1000-Å region, although previous fluorescense experiments have shown that considerable plasma resonance radiation is emitted.[38] Thus, any information on the ground states, or the resonant energy states of these atoms, i.e., the 4*s* configurations of Ar I, Ar II and Ar III and the 3*d* configurations of Ar II and Ar III, must be inferred indirectly from other data.

The principal results of the spectroscopic survey are that: (1) emission lines originating from high- and low-lying Ar II states dominate the spectra over the range $0 < z < 36$ cm; (2) weak lines of Ar I, observed throughout the flow field, begin to dominate the Ar II radiation for $z \gtrsim 40$ cm; (3) low-intensity radiation from low-lying states of Ar III can be found near the anode plane ($z < 2$ cm); (4) only weak impurity radiation, from W II, is observed.

These qualitative results support the presumed three-body recombination process. The rapid disappearance of Ar III downstream of the anode, along with the intense Ar II radiation from upper excited states, which at the prevailing electron temperature and density cannot arise from electron impact excitation, are compatible with the stream-wise progress of three-body recombination kinetics involving Ar III and two free electrons, yielding highly excited states of Ar II. Indeed, the observed relaxation length for the upper-state Ar

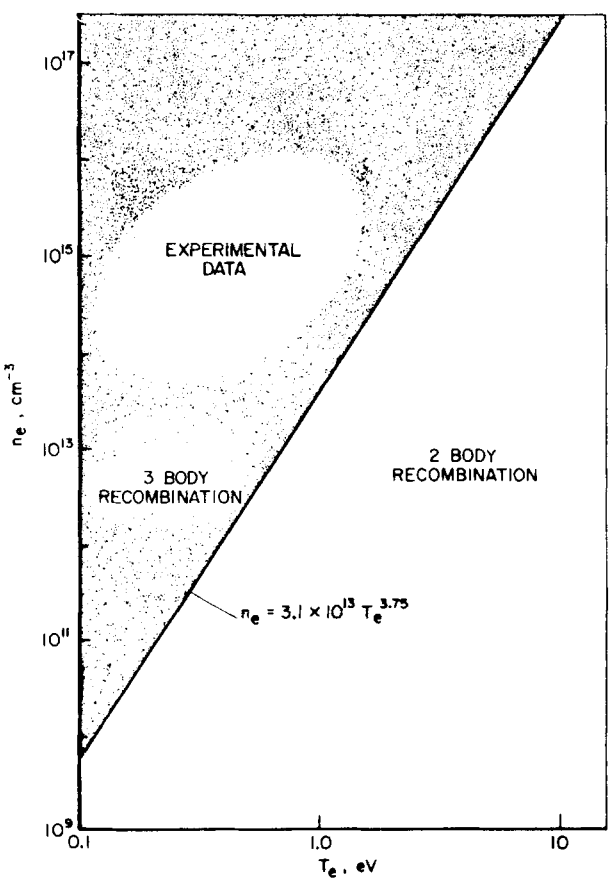

FIG. 12. Two- and three-body recombination regions.

II radiation of about 40 cm is consistent with the calculated recombination rate for this process at the prevailing conditions.

The appearance of the weak Ar I lines further downstream presumably indicates a similar recombination process of Ar II into neutral argon. However, photoelectric measurements of Ar I radiance show a time varying history, with considerable radiation emitted up to 100 μsec after the termination of the high-current arc, in contrast to that observed for Ar II (Fig. 8). The Ar I spectral lines thus may reflect the interaction of the arc plasma with background argon in the vacuum vessel.

F. Excited level population densities

Population densities of the excited electronic states may be determined from the absolute intensity measurements described earlier. These measurements concentrate on the excited levels of the argon first ion, with the exception of the 4*s* resonance level which emits far vacuum-ultraviolet radiation. Although this effort did not include vuv spectroscopic techniques, an estimate of the 4*s* population was obtained from the higher-density regions of the plume using the previously mentioned optical depth measurements.[38]

Since there are numerous substates associated with each electronic configuration, spectroscopic determination of the complete population distribution is not practical. A considerable simplification obtains, however, in that the various substates associated with most configurations can be shown to be thermalized at the electron temperature, i.e., the populations of the various states within the level are related by the Boltzmann factor. In these cases, the total configuration population can be determined from the local electron temperature and the density of a single configuration substate.

Using this strategy, the population distribution of the electronic states of Ar II have been determined at different locations in the exhaust flow. The distribution at an axial location of $z = 12$ cm is shown in Fig. 13. The strong coupling of the highly excited states above 6*s*′ to the free electrons is evident in the thermalization of these states with the continuum temperature T_e obtained from the slope of the

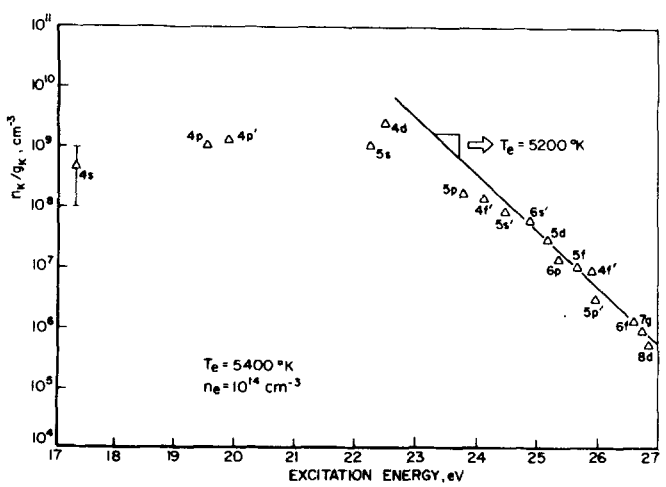

FIG. 13. Centerline Ar II state densities, $z = 12$ cm.

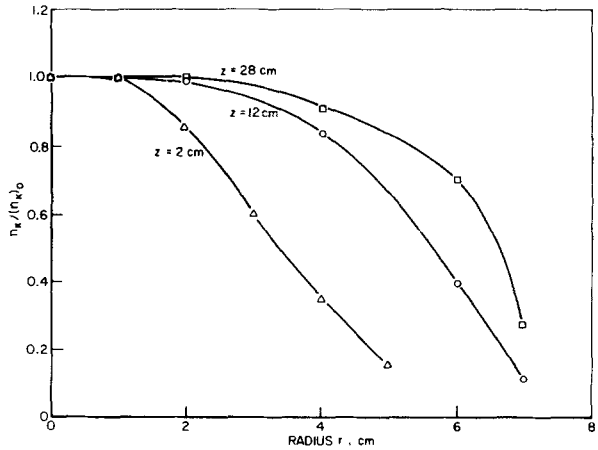

FIG. 14. Normalized population of $(^3P)4p\ ^3D^0_{3/2}$.

line through these states. This value, some 5200 ° K, is in good agreement with the probe data. The lowest-lying level in equilibrium with the free electrons, the so-called "bottleneck state", depends on the electron collisional rates and hence on n_e and T_e.[39] For example, in the vicinity of the anode, where the electron collisional rates exceed those at $z = 12$ cm, the bottleneck state has moved downward from the proximity of the 6*s*′ level to the more tightly bound 4*f*′ level.

At both positions, the more tightly bound states are observed to deviate from their Saha-Boltzmann values. Population inversions are evident between the 4*p* and 4*d* configurations. However, this must be interpreted with caution since the thermalization of the substates of the 4*d* level is incomplete due to the strong radiative coupling of some of these states to ground. Hence, the assignment of the mean population density of the 4*d* configuration is troublesome. A few of the low-lying 4*d* substates that are not strongly coupled to ground are indeed inverted with respect to high-lying 4*p* substates, but the inversion densities are not sufficient to allow laser oscillation.

In order to complete the excited population distribution, the 4*s* level density must be known. Since a line radiance technique is not possible, the absorption coefficient (loss or gain) of certain transitions between the 4*p* and 4*s* configurations was measured.[38] Although the uncertainties in this measurement are large due to the small value of the optical depth, overall gains of ~ 10% were obtained for the 4880-Å transition. With knowledge of the 4*p* configuration population from previous measurements, the optical depth measurement, which is proportional to the path integral of the density difference between the states, allows a crude determination of the average 4*s* population. The 4*s* configuration density obtained in this fashion is shown in Fig. 13, with the brackets reflecting the uncertainty in the measurement.

The excited stated populations are again consistent with the collisional-radiative recombination model of the MPD exhaust flow. The underpopulation of the low-lying energy states relative to their Saha-Boltzmann values is characteristic of a plasma in which the upper states are fed by the three-body recombination, while the lower states are radiatively depopulated. Because collisional deactivation of

the 4s level is inefficient due to the large energy spacing to ground, the existence of the 4p-4s inversion indicates little reabsorption of resonance radiation, and in view of the 10-cm plasma diameter over which the inversion prevails, a substantial underpopulation of the ion ground state is indicated.

The Ar II population density distribution at other axial locations up to $z = 30$ cm is similar to that of Fig. 13, except for the relative distribution of the 4p and 4s configurations. For axial locations where $n_e > 10^{14}$ cm^{-3} ($z < 12$ cm), no 4p-4s inversion is observed because of the rapid collisional deactivation of the 4p level to 4s and 3d states by electron impact.[40] Downstream of the 17-cm location, the inversion is maintained, but because the inversion density decreases due to the plasma expansion and the depletion of the Ar III reservoir, laser oscillation cannot be sustained.

III. LASING IN AN OPTICAL CAVITY

For a given population inversion to support laser oscillation, the small signal gain, which is proportional to the inversion density, must exceed a threshold value which takes into account both output coupling and undesirable losses in the resonator, e.g., diffraction losses. For a Doppler-broadened line at line center, this threshold value can be expressed as[41]

$$\int_0^L \Delta n_{ji}\, dx \geqslant -\left(\frac{2kT_+}{m_+}\ln 2\right)^{1/2} \frac{\nu_0^3}{c^3}\frac{8\pi}{A_{ji}}\ln(r_2)\,, \tag{3}$$

where the inversion density Δn_{ji} is given by

$$\Delta n_{ji} = n_j\left(1 - \frac{n_i g_j}{n_j g_i}\right) \tag{4}$$

and T_+ is the ion temperature, which is of the same order as the electron temperature, m_+ is the ion mass, r_2 is the reflectivity (in terms of electric field) of the output coupler, and the other quantities have the traditional spectroscopic connotations. In Eq. (3), the only loss mechanism that is considered is transmission through the output coupler, since diffraction losses, distributed losses, and absorption and reflection from the Brewster windows are negligible in this cavity.

To examine this condition for the 4880-Å 4p-4s inversion, the radial dependence of the inversion density must be known. Figure 14 shows the experimentally determined radial variation of the population of the upper state,

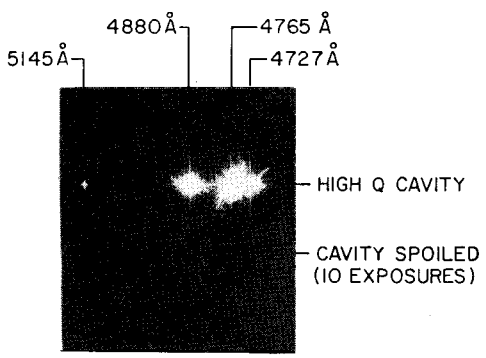

FIG. 15. Spectra of cavity output.

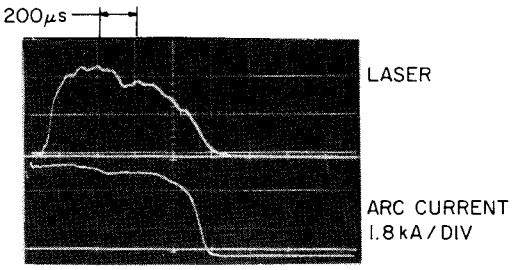

FIG. 16. Photomultiplier response to laser output at 4880 Å.

(^3P)4p $^2D^0_{5/2}$ normalized by its centerline value, with axial distance as a parameter. From Fig. 14, it can be seen that at the location of the maximum inversion density, $z = 12$ cm, the optical path length is approximately 10 cm. Using the $z = 12$ cm data, assuming constant density of the terminal level of the transition, the (^3P)4s $^2P_{3/2}$ state, integrating the left-hand side of Eq. (3) gives a value of 4.8×10^{10} cm^{-2}. This value is in good agreement with the results of the optical depth measurement. In comparison, the threshold value for lasing, calculated from the right-hand side of Eq. (3) using plasma ($T_i \simeq T_e$), atomic, and cavity properties, is 1.1×10^{10} cm^{-2}. Thus, at this location, a properly tuned cavity should oscillate.

Based on these measurements and calculations, the optical cavity described previously was installed transversely to the flow at an axial position 12 cm from the anode (Fig. 9). After adequate alignment and tuning, lasing was observed at the 5145-, 4880-, 4764-, 4727-, 4658-, 4579-, and 4545-Å lines of Ar II, all 4p-4s transitions. Figure 15 shows a spectrogram covering the wavelength range between 5150 and 4670 Å displaying the time-integrated radiance obtained from both a high-Q and a spoiled cavity. The starlike overexposure of the four spectral lines from a single discharge, shown in the upper part of Fig. 15, is typical of laser spectrograms. In contrast, the lower part of Fig. 15 shows the absence of any photographic response, even upon superposition of 10 discharges, when the reflecting mirror in the cavity is blocked.

Figure 16 shows the response of a Hamamatsu R818 phototube to the 4880-Å line in a calibrated detection system from which the time history of the radiance and the output power level may be determined. The lasing is seen to be nearly constant for the entire duration of the arc current pulse, indicating that quasi-cw operation has been obtained. The magnitude of this signal corresponds to an instantaneous output power of about 30 mW, whereas the total observed output power is approximately 200 mW. These power levels are in good agreement with those expected from the measured inversion density over the active medium volume utilized by the cavity.

To observe the dependence of the laser output on arc operating conditions, the current and mass flow have been varied from 2 to 21 kA and from 4 to 18 g/sec, respectively. No output from the cavity is detected for the lowest mass flow (4 g/sec) at any current. However, lasing is observed from 4 to 5 kA at 8 g/sec, from 4 to 6 kA at 12 g/sec, and weakly at 6 kA and 18 g/sec.

The limited range of operating conditions which yield lasing is evidence of the restricted set of plasma parameters capable of producing an adequate population inversion during rapid cooling in the downstream expansion. If the current is too low, the reservoir of Ar III for recombination pumping is inadequate. This situation also prevails if the mass flow is too high, with the added complication that the collisional relaxation rate may be too rapid to allow inversions to persist up to the axial station which is sampled by the resonator. For too high a current, and to a lesser extent for too low a mass flow, the absence of lasing may be attributable to higher local values of n_e and T_e because of the tighter constriction of the flow by the self-magnetic field pattern. The higher n_e and T_e erode the desired inversion, both by collisional deactivation and by the reduced recombination rate associated with the higher electron temperature.

IV. SUMMARY

The high-power quasisteady MPD arc has been shown to be capable of producing a highly ionized plasma jet which can be propitious for recombination lasing. In a particular domain of operation, electric probe measurements reveal that the electron temperature decays rapidly downstream of the arc chamber while the electron density remains sufficiently large so that recombination is mainly by three-body processes. The spectra show the flow to be dominated by the excited states of Ar II which, with the measured electron density and temperature, indicates that collisional-radiative recombination from Ar III prevails. Population density measurements in the expanding plasma flow show that the low-lying states of Ar II are underpopulated relative to their Saha-Boltzmann equilibrium values for the local plasma conditions. Population inversions between the $4p$ and $4s$ configurations, large enough to sustain laser oscillation, are detected 12 cm downstream of the accelerator for an arc curent of 4 kA and a mass flow of 12 g/sec. Using an optical cavity transverse to the plasma flow at this 12-cm downstream location, steady recombination lasing is observed photographically and photoelectrically in seven transitions between the $(^3P)4p$ and $(^3P)4s$ configurations. This lasing is observed to extend only over a very limited range of current and mass flow due to the simultaneous requirements for a sufficiently large reservoir of Ar III for adequate pumping, a rapid cooling in the exhaust flow to promote three-body recombination, and not too high an electron density to avoid collisional depopulation of the upper $4p$ level.

ACKNOWLEDGMENTS

This work was supported by NASA Grant NGL-31-001-005.

[1]L.I. Gudzenko and L.A. Shelepin, Zh. Eksp. Teor. Fiz. **45**, 1445 (1963) [Sov. Phys. JETP **18**, 998 (1964)].
[2]L.I. Gudzenko, L.A. Shelepin, and S.I. Yakovelenko, Sov. Phys. Usp. **17** (1975).
[3]V.F. Kitaeva, A.I. Odintsov, and N.N. Sobolev, Sov. Phys. Usp. 12, 699 (1970).
[4]D.R. Bates, A.E. Kingston, and R.W.P. McWhirter, Proc. R. Soc. London A **267**, 297 (1962).
[5]W.L. Bohn, 10*th International Conference on Phenomena in Ionized Gases*, edited by R.N. Franklin (Donald Parsons and Co., Oxford, England, 1971), p. 386.
[6]B. Gordiets, L.I. Gudzenko, and L.A. Shelepin, Sov. Phys.–JETP **28** (1969).
[7]W.L. Bohn, Appl. Phys. Lett. **24** (1974).
[8]D.D. McGregor and M. Mitchner, Phys. Fluids **17** (1974).
[9]*CRC Handbook of Lasers with Selected Data on Optical Technology* (Chemical Rubber, Cleveland, 1971).
[10]E.L. Latush and M.F. Sem, Sov. Phys.–JETP **37**, 1017 (1973).
[11]R.J. DeYoung, W.E. Wells, G.H. Miley, and J.T. Verdeyen, Appl. Phys. Lett. **28**, 519 (1976).
[12]G.W. Cooper and J.T. Verdeyen, J. Appl. Phys. **48**, 1170 (1977).
[13]W.T. Silfvast, L.H. Szeto, and O.R. Wood III, Appl. Phys. Lett. **31**, 334 (1977).
[14]V.A. Bhagavatula and B. Yaakobi (private communication).
[15]L.I. Gudzenko and L.A. Shelepin, Sov. Phys. Dokl. **10** (1965).
[16]V.M. Gol'dfarb, and G.A. Luk'yanov, Sov. Phys.–Tech. Phys. **13**, 10 (1969).
[17]W.L. Bohn and P. Hoffman, Z. Naturforsch. A **27**, 5 (1972).
[18]W.L. Bohn, *Gasdynamic and Chemical Lasers, Proceedings of the International Symposium*, 11-15 *October* 1976, edited by M. Fiebig and H. Hügel (DFVLR-Press Köln-Porz, Germany, 1976), p. 64.
[19]E.M. Campbell, R.G. Jahn, W.F. von Jaskowsky, and K.E. Clark, Appl. Phys. Lett. **30**, 575 (1977).
[20]A.C. Ducati, G.M. Giannini, and E. Muchlberger, AIAA J. **1**, 1452 (1964).
[21]R.R. John, S. Bennett, and J.F. Connors, Astronautica Acta, **11**, 97 (1965).
[22]H. Hügel, AIAA J. **6**, 1573 (1968).
[23]K.E. Clark and R.G. Jahn, AIAA J. **8**, 216 (1970).
[24]A.C. Malliaris, R.R. John, R.L. Garrison, and D.R. Libby, AIAA J. **10**, 121 (1972).
[25]M.J. Boyle, K.E. Clark, and R.G. Jahn, AIAA J. **14**, 7 (1976); **14**, 955 (1976).
[26]M.S. DiCapua and R.G. Jahn, AMS Report No. 1015, Princeton University, 1971 (unpublished).
[27]E.O. Johnson and L. Malter, Phys. Rev. **80**, 50 (1950).
[28]F.F. Chen, J. Nucl. Energy C **7** (1965).
[29]J.G. Laframboise, UTIAS Report 100, University of Toronto, 1966 (unpublished).
[30]R.G. Jahn, W.F. von Jaskowsky, and K.E. Clark, AMS Report 634y, Princeton University, 1975 (unpublished).
[31]H.R. Griem, *Plasma Spectroscopy* (McGraw-Hill, New York, 1964).
[32]D.R. Bates and A. Damgaard, Phil. Trans. R. Soc. London A **242**, 14 (1949).
[33]L. Minnhagen, Arkiv Fuer Fysik **25**, (1963).
[34]H. Kogelnik and T. Li, Appl. Opt. **5**, 1550 (1966).
[35]L.P. Pitaevskii, Sov. Phys.–JETP **1**, 919 (1962).
[36]Ya. B. Zel'dovich, and Yu. P. Raizer, *Physics of Shock Waves and High-Temperature Hydrodynamic Phenomena* (Academic, New York, 1966).
[37]A.R. Striganov and N.S. Sventitskii, *Tables of Spectral Lines of Neutral and Ionized Atoms* (IFI/Plenum, New York, 1968).
[38]E.M. Campbell, W.F. von Jaskowsky, K.E. Clark, and R.G. Jahn, AIAA Paper 75-852, AIAA 8th Fluid and Plasmadynamics Conference, Hartford, Conn., 1975.
[39]C.J. Chen, J. Chem. Phys. **50** (1969).
[40]P.L. Rubin and N.N. Sobolev, Sov. Phys.–JETP **41**, 848 (1975).
[41]A. Yariv, *Introduction to Optical Electronics* (Holt, Rinehart and Winston, New York, 1971).